P1.35 MESO-SCALE PRESSURE DIPS

ACCOMPANIED BY A SEVERE CONVECTIVE STORM OF TROPICAL CYCLONES

Hironori Fudeyasu*, Satoshi Iizuka, and T. Matsuura

National Research Institute for Earth Science and Disaster Prevention

1. Introduction

Fujita (1952) first described the phenomenon of a pressure dip that is occasionally observed in association with typhoons crossing the Japan Islands or moving along the southern coast of Japan (Fujita 1952, 1992; Nakajima et al. 1980; Fujii 1992; Maeda 1994; Fudeyasu and Tsukamoto 2000). The occurrence of a pressure dip is generally only recognized by analysis of barograph data. Figure 1 shows the time series data of surface wind direction and speed, temperature, dew-point temperature, and pressure recorded at station K (see Fig. 3) during the passage of Typhoon Zeb. A pressure dip, consisting of a rapid decrease and subsequent increase in surface pressure for 1500-1530 UTC, is distinct from the gradual decrease in surface pressure recorded during the passage of typhoon center. The previous studies show that pressure dips are meso-β-scale phenomena with a band-like structure and typical dimensions of 150 km by 50 km. The maximum observed amplitude of pressure dips is 7-9 hPa, and the duration recorded at a single station is always less than one hour. Pressure dips are accompanied by severe convection, causing sometimes the severe damages at various locations over the Japan Islands. It was reported that, for example, there was extensive damage resulting from instantaneous wind speed of 54.3 m s^{-1} within a pressure dip associated with Typhoon Mireille (Maeda 1994; Fujita 1992). They appeared on the left side of the typhoon center, although strong winds associated with typhoons are generally observed on the right side of typhoon center.

The formation process of pressure dips remains poorly understood. Matsumoto and Okamura (1985) used Doppler radar data and surface observations to study a pressure dip observed over Japan during the passage of Typhoon Gay, and concluded that the pressure dip was due to the passage of an internal gravity wave excited via decay of the typhoon. Tsujimura (1993) concluded that the pressure dip associated with Gay was rather due to a solitary internal gravity wave. In contrast, Inoue et al. (1999) argued that a pressure dip observed within Typhoon Zeb was a low-pressure region formed behind the gust front of a gravity current caused by an intense rain band. It is apparent that the formation process of pressure dips is a controversial issue.

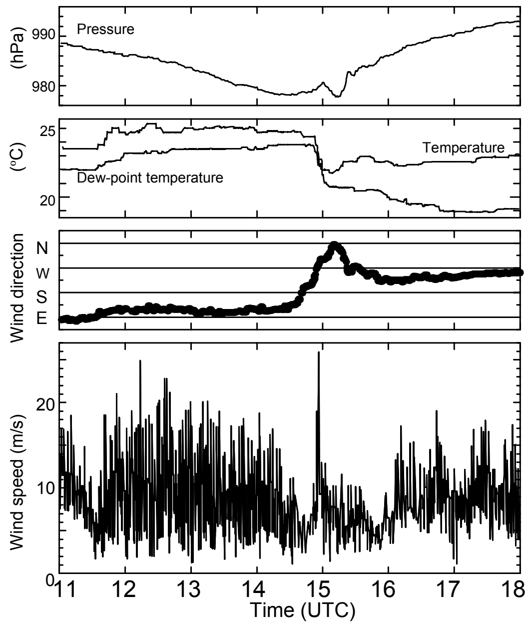

Fig. 1. Record of surface pressure, temperature, dew-point temperature, and wind speed and direction as observed at station K from 1100–1800 UTC on 17 October 1998. See Fig. 3 for location of station K.

In this study, we first examine the process of pressure dip formation using a high-resolution numerical model. We focus on the pressure dips associated with Typhoon Zeb, because the track is most suitable for investigating the structure and occurrence of pressure dips by using available comprehensive observational data. The model successfully reproduces the major features of the pressure dip with Zeb. We then attempt to clarify the formation process of pressure dips.

2. Data and Model

2.1 Data

Tracks of typhoons were obtained from the best-track archives of the Regional Specialized

*Corresponding author address: Hironori Fudeyasu, National Research Institute for Earth Science and Disaster Prevention , Tennodai 3-1, Tsukuba, Ibaraki 306-0006, Japan; E-mail: fude@bosai.go.jp

Meteorological Centers (RSMC) Tokyo–Typhoon Center. The dataset consists of the names, positions, maximum surface pressure, and maximum wind speeds of typhoons, generally recorded at 6-hour intervals. Estimates of the hourly positions of typhoon centers were determined by linear interpolation of the 6-hour data.

An hourly rainfall patterns are estimated from the Radar–Automated Meteorological Data Acquisition System (AMeDAS) data provided by the JMA. The Radar–AMeDAS data is an hourly averaged rainfall analysis created from a composite of observations from operational precipitation radars and the AMeDAS data (Obayashi, 1991). The Radar-AMeDAS data during the period April 1988 to March 2001 has a horizontal resolution of 5 km.

Details of the large-scale atmospheric conditions around the typhoons with pressure dips were reconstructed from reanalysis data, sourced from the National Centers for Environmental Prediction–National Center for Atmospheric Research (NCEP–NCAR), with 6-hour intervals covering the period 1980 to 1998 and a horizontal resolution of 2.5° (Kalnay et al. 1996). Infrared satellite images from the Japanese Geostationary Meteorological Satellite (GMS) spanning the period 1980-1998 are also used.

2.2 Model

A numerical simulation was performed using the Mesoscale Model 5 (MM5) ver. 3.5 jointly developed by Pennsylvania State University and the NCAR. MM5 is a non-hydrostatic model developed as a community mesoscale model (Dudhia 1993; Grell et al. 1995). The model incorporates multiple nested grids and includes both explicit moist physical processes and cumulus parameterization schemes. This model solves the nonlinear, primitive equations using Cartesian coordinates in the horizontal and terrain-following sigma coordinates in the vertical. Pressures at sigma levels are determined from a reference state that is estimated using the hydrostatic equation from the given sea level pressure and temperature of standard lapse rate.

In this study, the model contains 30 sigma levels of fine resolution near the surface, while the top of the model is at 50 hPa. The simulation was conducted using two domains as shown in Fig. 2. The outer domain (D1) has 271 × 271 grid points, centered at 33ºN, 133ºE, with a horizontal resolution of 15 km. The inner domain (D2) has 460 × 460 points with a horizontal resolution of 5 km. D1 is designed to produce the initial and boundary conditions for D2, while D2 is designed to resolve explicitly the fine structures of typhoons and associated pressure dips. We also conducted the simulation using a horizontal resolution of 3 km, but the results are essentially similar to those with a horizontal resolution of 5 km.

The simple ice scheme (Dudhia 1989) is used as cloud microphysics. In this scheme, cloud water and rainwater below 0 ºC are treated as cloud ice and snow respectively. The convective scheme of Grell (1993) is used as a cumulus parameterization except D2. The model also includes the planetary boundary layer (Hong and Pan 1996), a five-layer soil model, and a cloud-radiation interaction scheme (Dudhia 1989, 1993; Grell et al. 1995).

The initial and lateral boundary conditions of D1 for the simulation of Typhoon Zeb are derived from the Global Asian Meteorological Experiment (GAME) reanalysis dataset produced by the Meteorological Research Institute–JMA (http://gain-hub.mri-jma.go.jp/GAME_reanal.html). The dataset includes the 3-dimensional analyzed atmospheric fields over the Asian and Pacific regions (30ºE–180º, 80ºN–30ºS), covering the period from April to October 1998. The data have a horizontal resolution of 0.5° for both longitude and latitude, with 17 vertical levels and a 6-hour time interval. Sea surface temperature is represented by the skin temperature of the NCEP–NCAR reanalysis dataset (Kalnay et al. 1996).

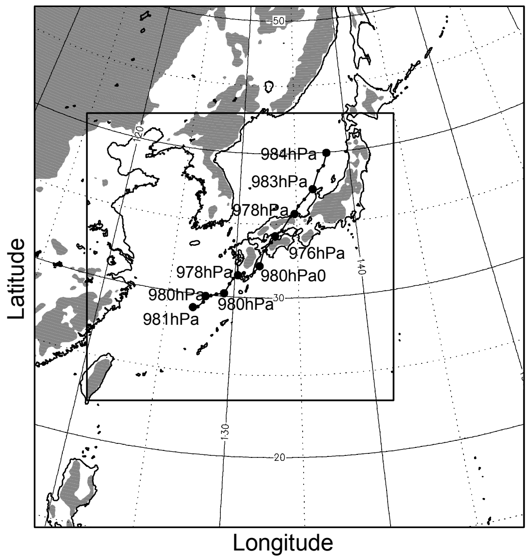

Fig. 2. Model domains of the numerical simulations and terrain. The regions higher than 400 m is shaded. Track (line) and 3-hourly locations (closed circles) of simulated typhoon derived from the domain 2 simulation during the period 0000 UTC on 17 to 0000 UTC on 18 October 1998.

The simulation of D1 was performed for 42 hours, starting at 1800 UTC on 16 October 1998, after the model was integrated for 18 hours during an initial spin up from 0000 UTC on 16 October. During the initial spin-up, the continuous dynamical assimilation where forcing function are added to the governing model equations to gradually “nudge” the model state toward the reanalysis data for only wind components (Grell et al. 1995). The relaxation boundary conditions are adopted as the lateral boundary conditions (Anthes et al. 1987), in which the model-predicted values are relaxed to those estimated from large-scale analysis data. The D2 simulation began at 0000 UTC on 17 October 1998, and was performed for 36 hours using the initial and boundary conditions interpolated from the results of the D1 simulation. At the start of the D2 simulation, the center of Typhoon Zeb was located to the southwest of Kyushu (Fig. 2).

3. Pressure dip associated with Typhoon Zeb

3.1 Features of observed pressure dip

Typhoon Zeb was upgraded to a tropical storm (maximum 1 minute sustained wind speed in excess of 17.2 m s^{-1} or 35 knots) from a tropical depression at 11 October 1998 when situated at 10ºN, 140ºE (Fig. 3). The typhoon turned toward the northwest over the vicinity of the Philippine Sea and increased in intensity to that of a Super Typhoon (maximum 1 minute sustained wind speed in excess of 70 m s^{-1} or 135 knots). The typhoon made landfall in Kyushu at 0700 UTC on 17 October, with a central pressure of 975 hPa and a maximum wind speed of 25 m s^{-1}. The typhoon then passed over Shikoku and the main island of Japan, at 1400 UTC on 17 October. After reaching the Japan Sea, Zeb moved north-northeast and eventually weakened. It was downgraded to an extratropical cyclone when located near Hokkaido at 0000 UTC on 18 October.

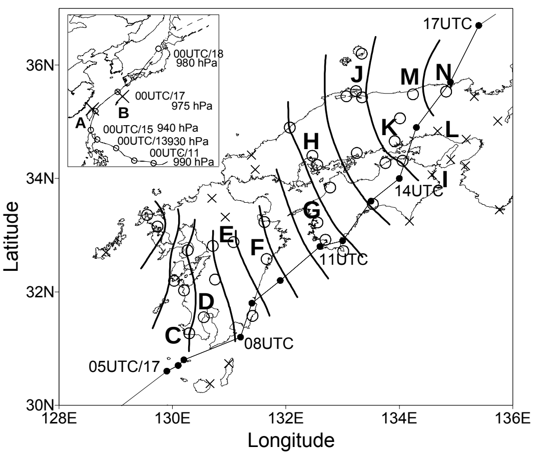

Fig. 3. Hourly locations of pressure dip axis (solid lines) for Typhoon Zeb (black circles). Open circles indicate stations where the pressure dip was observed, whereas crosses indicate stations that failed to record the pressure dip.

During the passage of Zeb through the Japan Islands, a considerable decrease and subsequent increase in surface pressure was recorded at several meteorological stations. Figure 4 shows time series data of surface pressure recorded by barographs at the meteorological stations. In addition to a gradual change in surface pressure related to the passage of Zeb, a sudden 3-8 hPa drop in surface pressure is discernable. The pressure dips appear a few hours after the passage of the typhoon center for all stations except J, where a pressure dip was recorded prior to the arrival of the typhoon center. It should be noted that the pressure dip exists only to the northwest of Zeb as it tracked to the northeast (Fig. 3). There is no signal of a pressure dip at stations I and L located to the southeast of the typhoon. A pressure dip was also not observed on the northern part of Kyushu and Chugoku distinct during the period from 0800 to 1200 UTC, indicating the extent of the pressure dip axis that is defined by isopleths of the minimum pressure within the pressure dip. Although most meteorological stations recorded the pressure dips after the passage of the typhoon center, a number of stations far away from the typhoon center recorded a pressure dip in advance of the typhoon center during the period 1300 to 1500 UTC. Station A, located to the northwest of the typhoon track (Fig. 3), recorded no signal of a pressure dip. We interpret this to indicate that the pressure dip axis did not extend to lower latitudes.

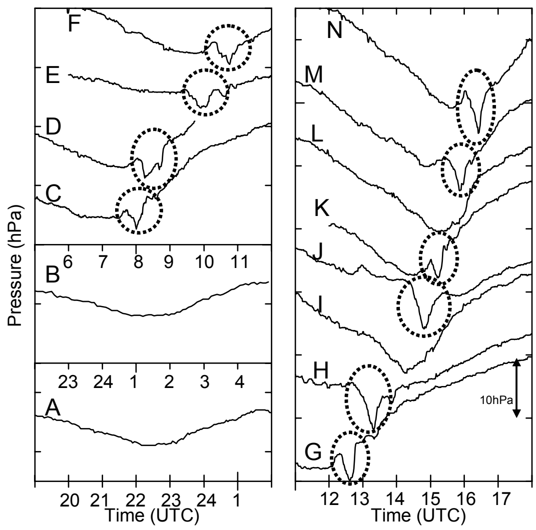

Fig. 4. Barograph charts recorded at meteorological stations during the passage of Typhoon Zeb from 16–17 October 1998. Locations of stations are indicated in Fig. 3. Detection of pressure dip at each station is indicated by dashed circles.

The arrival of the pressure dip was accompanied by a sudden change in the surface winds (Fig. 1), although these wind changes were not observed at all meteorological stations because of local effects such as mountainous terrain. Wind speed weakened after the passage of the typhoon center, but strong winds were observed immediately prior to the arrival of the pressure dip. Station K was located to the left side to moving direction of Zeb, and would therefore be expected to record an anti-clockwise change in wind direction with the passing of the typhoon. The wind direction, however, recorded a clockwise change for the 30 minutes prior to the arrival of the pressure dip.

The approach of the pressure dip was also accompanied by rapid changes in surface temperature and dew-point temperature, which fell 3ºC an hour before the pressure dips appeared (Fig. 1). These trends were observed only at stations near the track of the typhoon. The thermal changes are considered to be related to the surface fronts associated with Zeb rather than the pressure dip itself (not shown). Fujita (1952) documented no significant change in surface temperature associated with a pressure dip. At a few hours before a pressure dip appears, however, the surface temperature and dew-point temperature at some meteorological stations recorded a sudden decrease (see also Fig. 1 of Fujita 1952, Fig.4 of Matsumoto and Okamura 1985, Fig. 3 of Fujii 1992, and Fig. 2 of Maeda 1994). As stated above, these thermal changes appear to be related to the fronts combined with the typhoons rather than the pressure dip. This topic will be discussed in more detail later.

Figure 5 shows an hourly rainfall amount derived from the Rader-AMeDAS data at 0700, 0900, 1300, and 1500 UTC on 17 October 1998. Intense rainfall precedes the arrival of the pressure dip axis. The rainfall was weak at the center of the pressure dip and stopped with the passing of the pressure dip axis. The AMeDAS data, which contains a record of surface wind, temperature and rainfall averaged over 10-minute intervals since 1995, shows that the rainfall changes occurred abruptly over a period of less than 30 minutes (not shown).

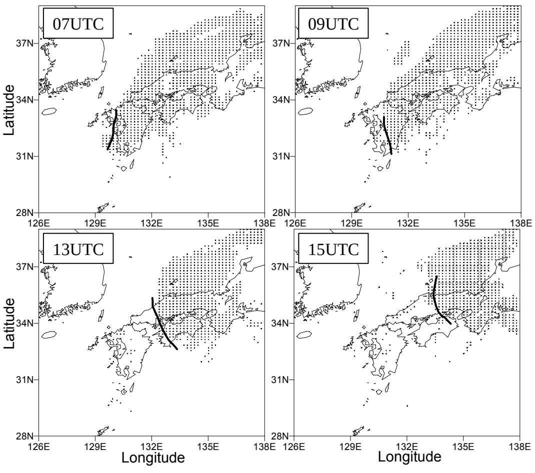

Fig. 5. Rainfall region more than 1 mm hour^{-1} derived from the Rader-AMeDAS data and the pressure dip axis at 0700, 0900, 1300, and 1500 UTC on 17 October 1998. The solid lines denote the location of the pressure dip axis.

3.2 Validation of simulated pressure dip

We here validate the features of the Typhoon Zeb simulation. The track of Zeb simulated in the D2 with a finest resolution, determined from the area of minimum sea level pressure of the simulated typhoon, is shown in Fig. 2. The simulated typhoon track is generally in good agreement with the observed typhoon track (Fig. 3). The central pressures of the simulated typhoon are about 980 hPa during 17 October when the typhoon passed over Kyushu, Shikoku, and the Main Island of Japan before reaching the Japan Sea. The pressures recorded within the centre of Zeb at this time are 975-980 hPa. The track of the simulated typhoon, however, is delayed by an hour in comparison with the movement of Zeb. This is because the initial position of D2 is shifted westward due to the insufficient simulation of the D1 with a coarse resolution. This discrepancy may be related to a bias in the boundary conditions or in the assimilation used in the present model. Although the arrival time of the simulated typhoon differs from actual observations, the track and intensity of Typhoon Zeb are well reproduced by the model.

We next compare the simulated pressure dips with those observed within Zeb. Figure 6 presents time series data of the simulated sea level pressure at 3-minute intervals at each station (see Fig. 3). Portions of the time series data at stations A and B are not shown because the typhoon center had passed over these stations prior to the initial time of the D2 simulation at 0000 UTC on 17 October (Fig. 2). Also note that the locations of stations H, I, J, K, L, M, and N have been shifted 1º westward from actual locations to accommodate

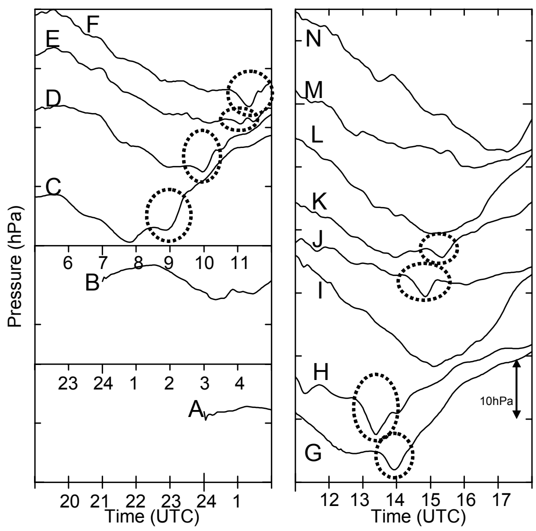

Fig. 6. Simulation time series data of the sea-level pressure at meteorological stations during the passage of a typhoon from 16–17 October 1998. Locations of stations are indicated in Fig. 3. Detection of pressure dip at each station is indicated by dashed circles.

differences in the simulation and observational data for the period after Zeb made landfall over Shikoku.

The time series data of simulated sea level pressure records a dip-like decrease in sea level pressure associated with the passage of the typhoon center, although the amplitudes are generally smaller than the observations (Fig. 4). The peak of the pressure dip is recorded at station C at 0900 UTC, station D at 0955 UTC, station E after 1050 UTC, station F at 1115 UTC, and station G at 1355 UTC. The pressure dips generated within the simulation occur about an hour after the observed pressure dip was recorded at each station. This time discrepancy occurs because the track of the simulated typhoon is one-hour late compared with the track of Zeb (Fig. 2). A pressure dip of 6 hPa was recorded at station H at 1315 UTC, and pressure dips were also recorded at station J at 1445 UTC and station K at 1515 UTC. These times are comparable to the timing of the actual pressure dips observed at each station. As in the observational data, there is no signal of a pressure dip at stations I and L. In contrast to observational data, the simulated pressure dip is not recorded at stations M and N, although the reason is not clear.

Figure 7 shows time sequence data of the simulated sea level pressure from 0500 to 1800 UTC on 17 October 1998, together with the simulated an hourly rainfall. At 1300 UTC, when the typhoon center is located over western Shikoku (Fig. 7d), a low-pressure region distinct from the typhoon center extended toward the north from an area west of the typhoon center. This low-pressure region corresponds to the pressure dip axis as defined by isopleths of the minimum pressure within the pressure dip. The passage of the pressure dip axis can be traced by a sudden decrease and then increase in the simulated sea level pressure recorded at several stations (Fig. 6). The pressure dip has a length of 200 km and width of 50 km, which is consistent with the dimensions derived from observational data (Fig. 3). It is also noted that, as in the observation (Fig. 5), intense rainfall exceeding 20 mm per hour interval precedes the arrival of the simulated pressure dip axis. The simulated rainfall is weak at the center of the pressure dip and stopped with the passing of the pressure dip axis, which is consistent with the rainfall features derived from observational data (Fig. 5).

The simulated pressure dip is not recorded prior to 0500 UTC (Fig. 7a), but develops in the northwest quadrant of the typhoon from 0800 UTC (Fig. 7b) when the typhoon center is located over the sea to the southwest of Kyushu. This indicates that formation of the pressure dip is not related to the topography of the Japan Islands (Fig. 2). The pressure dip axis then moves northeast with the typhoon, and extends further from an area west of the typhoon center (Fig. 7c). The pressure dip is most clearly discernable at 1300 UTC (Fig. 7d). As the typhoon moves further northeast, the pressure dip breaks down (Figs. 7e and f), and is not recorded at stations M and N (Fig. 6).

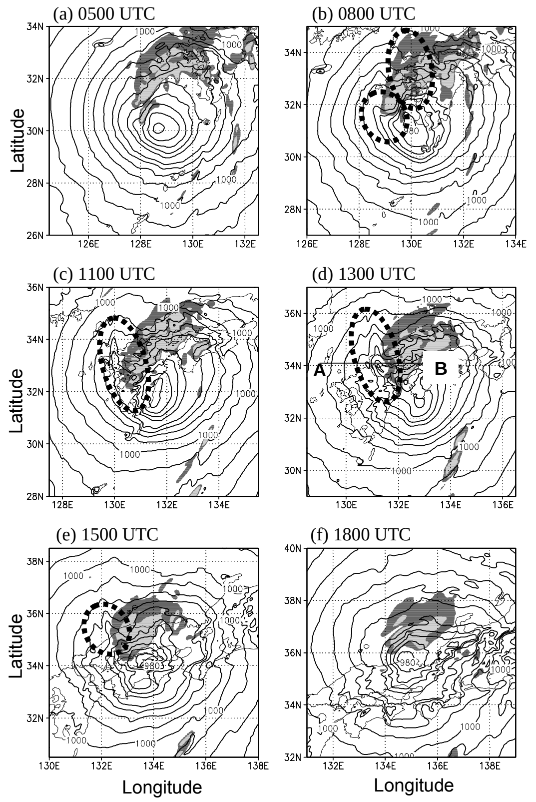

Fig. 7. Simulation sea-level pressure fields and hourly rainfall within domain 2 at (a) 0500, (b) 0800, (c) 1100, (d) 1300, (e) 1500, and (f) 1800 UTC on 17 October 1998. Contours interval is 2 hPa. Detection of pressure dip axis is indicated by dashed circles. Regions of rainfall greater of 10-20 mm hour^{-1} are heavily shaded, while grater than 40 mm hour-1 are lightly shaded.

Although the amplitude of the simulated pressure dips is weaker than the observations, the features of the simulated pressure dip are sufficiently similar to that of the observed pressure dip that we can confidently use the simulation data to investigate the processes of pressure dip formation.

3.3 Structure of simulated pressure dip

Figure 8 shows vertical sections of potential temperature anomaly at each pressure level across the station H at 1300 UTC (see. Fig. 7d), together with the sea level pressure. The potential temperature anomaly was calculated as the deviation from the average temperature of the entire D2 area. The upper troposphere contains warm anomalies associated with the warm core of the typhoon, and resulting in a broad lowering in sea level pressure. In the lower troposphere below 700 hPa, warm potential temperature anomalies exist east of 132ºE due to a northward warm advection associated with cyclonic circulation, while the anomalies are relatively cool to the west of 132ºE. At 131.5ºE, within the colder region in the lower troposphere, there exist remarkable warm potential temperature anomalies from 700 to 900 hPa that correspond to a dip in the sea level pressure.

Figure 9 shows vertical sections of vertical velocity, relative humidity with winds in the plane, rain water/snow mixing ratio, and cloud water/ice mixing ratio, respectively, as same in Fig. 8. Near the typhoon center, there is a relative wet region accompanied by the strong ascending flow through the entire troposphere (Figs. 9a and b). Over the pressure dip region immediately west of the ascending flows is a local strong descending flow from 300 hPa down to the surface, accompanied by the wave-like vertical circulation to the rear. In association with the strong descending flow, there is the relative dry region below 600 hPa in the same narrow region as the warm potential temperature anomalies. The dry region is connected with a dry region in the upper and middle troposphere accompanied by the westerly winds.

At the higher altitude, ice water is advected outward from the typhoon center, forming the overhanging anvil over the pressure dip region (Fig. 9c). This ice water in the anvil aggregates and grows a snow as they approach the 0 ºC level (Fig. 9d). It is noted that, in the present simulations, cloud water and rainwater below 0 ºC are treated as cloud ice and snow respectively, as cloud microphysics (Dudhia 1989). Therefore, when they fall through the 0 ºC level, they melt and fall to the ground as rain. It results to that the concentrations of snow are abundant above the melting level while there is few cloud water below the melting level. The pressure dip is found below the overhanging anvil. These pictures imply that the pressure dip is linked to the warm potential temperature anomalies in the lower troposphere, accompanied by the intrusion of an upper dry air mass due to the strong local descending flow.

4. Formation processes of simulated pressure dip

4.1 Heat budget

We now consider how the warm potential temperature anomalies in the lower troposphere form. The process of anomaly formation can be investigated by describing the anomalies in terms of a thermodynamic equation. The time tendency of potential temperature is estimated by the difference in the potential temperature sampled at a time interval of 3 minutes. The diabatic term, including radiation, diffusion, and net heating related to phase changes of water, is defined as the residual derived from both horizontal and vertical advection terms and the time tendency.

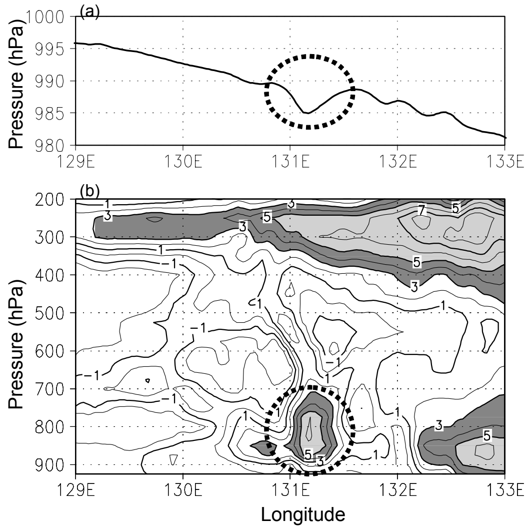

Fig. 8. Cross-section of (a) sea level pressure and (b) potential temperature anomalies at 1300 UTC on 17 October 1998. Location of cross-section is marked as line AB in Fig. 8(d), at the latitude of 34.1ºN. Contour interval is 1 K. The region of anomalies of 3-5 K are heavily shaded, while anomalies > 5 K are lightly shaded. Detections of warm potential temperature anomalies related to a pressure dip and pressure dip are indicated by dashed circles.

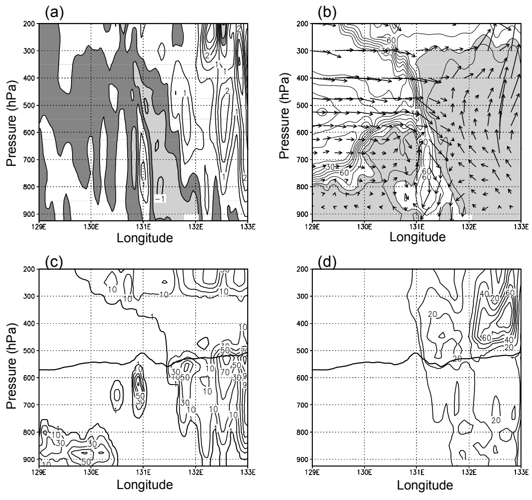

Fig. 9. Same cross-sectional profiles as in 9 except for (a) vertical velocity, (b) relative humidity and horizontal winds (m s^{-1} arrows, scale at bottom left), (c) water/snow mixing ratio, and (d) cloud water/ice mixing ratio. (a) Contour interval is 0.5 m s^{-1} and dark and light shading represents areas of vertical velocity less than 0.0 and –0,5 m s^{-1}, respectively. (b) Contour interval is 10 % and the region grater than 80 % is shaded. (c) Contour interval is 2.0 * 10^{-5} kg kg^{-1} and (d) 1.0 * 10^{-3} kg kg^{-1}. The solid line indicated the level of 0 C.

The rapid decrease in surface pressure appears at station H from 1245 to 1330 UTC (Fig. 4), coinciding with the development of warm potential temperature anomalies in the lower troposphere. The thermodynamic balance shows that the warming in the low level from 1315 to 1330 UTC is caused mainly by vertical advection (Fig. 10). Although the cooling due to diabatic term contributes to partly counteract the warming, the adiabatic warming of descent in the low level is not balanced by the diabatic cooling. The cooling due to horizontal advection term accompanied by the cyclonic circulation is relatively small in the low level. This indicates that the adiabatic descent of air is responsible for the formation of warm potential temperature anomalies in the lower troposphere. At the level above 600hPa, however, the warming due to vertical advection is mostly balanced by diabatic term. The warming at 400hPa results from the outflow of warmer air from the typhoon center, while the cooling at 550hPa seems to be related to the inflow of environmental air with lower potential temperature by westerlies.

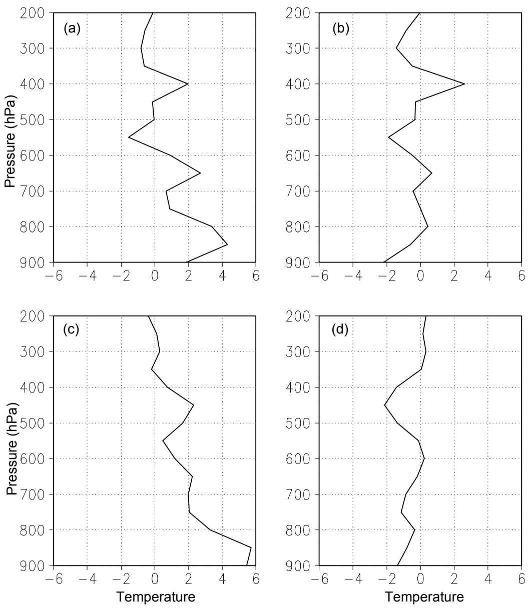

Fig. 10. Vertical profiles of (a) time tendency of potential temperature, (b) horizontal advection of potential temperature, (c) vertical advection of potential temperature, and (d) diabatic effect on potential temperature at station H for period 1315-1330 UTC on 17 October 1998.

4.2 Trajectory analysis

In order to clarify the formation of the warm potential temperature anomalies in the lower troposphere furthermore, we conducted a backward trajectory analysis using three-dimensional winds sampled at 3-minute intervals. Initially, 80 parcels were defined uniformly in the levels from 700 hPa over the surrounding area of station H (131.5ºE–132.0ºE, 34.0ºN–34.7ºN) at 1300 UTC. This region includes both the pressure dip axis and surrounding areas. Figure 11 shows the trajectories of the parcels over the next 12 hours. The origins of the parcels that resided over the pressure dip can be traced back in time to the eastern coast of China (Fig. 11a), while the parcels in the surrounding area originated from the east-northeast and to a lesser degree from the south (Fig. 11b).

Figure 12 presents time series data of several averaged quantities of parcels that originated from the west (western parcels), which were released initially 700 hPa level over the surrounding area of station H. Also shown in the figure are the time series data of parcels that originated from the east-northeast (eastern parcels), which were initially situated slightly east of the station H. The eastern parcels remain below 3000 m in the colder region over the northern coast of Main Island of Japan until 1000 UTC (Figs. 11b and 12a). At 1000 UTC the eastern parcels are brought into the typhoon center and ascend to 3000 m. The potential temperature and equivalent potential temperature increase with the moist-adiabatic lapse rate (Fig. 12b).

The western parcels can be traced back to the upper level around 10000 m (above 300 hPa) at 0100 UTC (Fig. 12a). Up until 1030 UTC, strong upper-level westerly winds propel the western parcels to the east-northeast (Fig. 11a) on the gently descending slope of the isentropic surface within the upper troposphere. The western parcels conserve potential temperature and equivalent potential temperature (Fig. 12b), and subsequently low humidity (Fig. 12d). The initial motion of the western parcels is thus predominantly adiabatic. Once the western parcels have overtaken the northeastward moving typhoon, during 1030 to 1300 UTC, they move rapidly downward from 8000 to 3000 m within the intense descending flow (Figs. 12a and c). During this period, the water mixing ratio of the western parcels increases along with relative humidity (Fig.12d), indicating that water is supplied from the wet region of the typhoon. Although the mixing ratio of the western parcel increases, the equivalent potential temperature remains steady as the potential temperature decreases during 1030 to 1200 UTC (Fig. 12b). This indicates that evaporative cooling is operates through the subsidence. From 1245 to 1345 UTC when the pressure dips appears at the surrounding area of station H, the changes in potential temperature, humidity and water mixing ratio are small, suggesting that evaporative cooling is insufficient to offset the adiabatic warming there, because there is less hydrometer in the low levels below the melting level. Then, the western parcels are 4 K higher than the eastern parcels (Fig. 12b).

The above trajectory analysis suggests that downdraft which is a local strong descending flow over the pressure dip) plays an important role for the formation of a pressure dip. As a typhoon moves into the mid-latitude westerlies, a dry air associated with the westerlies enters into a typhoon with a wet air. The interaction between typhoon circulations and westerly winds forms the equivalent potential temperature fronts at the mid level, while the overhanging anvil is evident at the upper level. Then, a dry air entering just below anvil is cooled by evaporation and becomes negative buoyancy, producing downdraft. Namely, the formation of a mesoscale downdraft results from evaporative cooling of dry air masses carried by upper-level westerly winds toward the wet typhoon region (Figs. 12e and f). The downdraft has its peak at 1215 UTC (Fig. 12c) when the parcels reach around the melting level (Figs. 9c and d). The parcels undergo acceleration through evaporation and melting until it goes through the melting level. After it goes beyond the melting level, evaporative cooling becomes insufficient to offset the adiabatic warming, because there is no sufficient water in the low level (Figs. 9c and d). As a result, warm potential temperature anomalies appear in the low level, causing a pressure dip. The horizontal scale of pressure dips is set by the width of the region of mesoscale downdraft around the melting level. The warming in the low level causes parcels to become positive buoyancy, resulting in the deceleration of downdraft in the low level (Fig. 12c). It is noted that the downdraft impinging on the low levels excites the gravity waves on the rear side (Figs. 9a and b), but the induced surface pressure change is much weaker that that caused directly by downdrafts (Fig. 8).

6. Discussion

The present study suggests that the formation process of a pressure dip is similar to that of a wake low (e.g., Johnson and Hamilton, 1988). A wake low generally appears near or just behind of squall lines, in association with warming by unsaturated descent. The strong descending flow playing a role in the formation of the warming is connected the subsidence to rear inflow into the squall line (Johnson and Hamilton, 1988). Previous studies relevant to the wake low propose several ideas regarding the causes of the strong descending flow (Miller and Betts 1977; Johnson and Hamilton 1988; Zhang and Gao 1989; Schmidt and Cotton 1990; Gallus 1996). In addition, it is suggested that the environmental flow in which the squall line occurs determines the intensity of rear inflow into the squall line at middle and upper level.

In the case of pressure dips, the mid-latitude westerlies corresponded to rear inflow are extremely strong, while many cases of wake low have weaker rear inflow into the squall line at middle and upper level. The mid-level convergence of typhoon circulation and mid-latitude westerlies is linked to the formation of a steep upward-sloping westward front at mid level where effectively the intense downdraft is caused. A pressure dip therefore appears by which the intense mid latitude westerly affects typhoons.

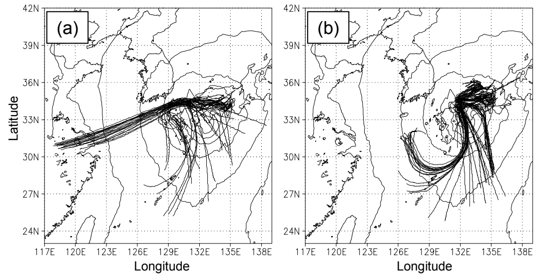

Fig. 11. Trajectories of 80 parcels over 12 hours for period 0100–1300 UTC on 17 October 1998. The origins of the parcels are at 700 hPa level (a) over the pressure dip axis, and (b) over surrounding areas.

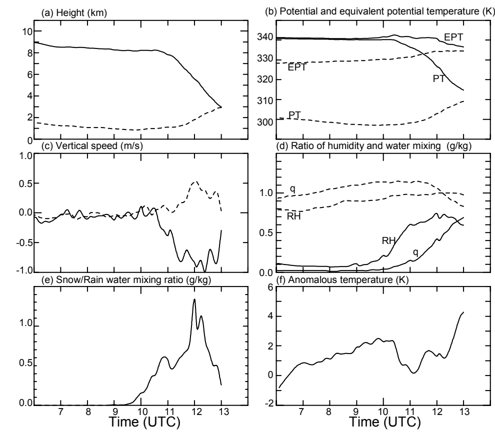

Fig. 12. Time series data of averaged several parameters of the western (solid line) and eastern (dashed line) parcels for period 0100–1300 UTC on 17 October 1998. (a) Height, (b) potential temperatures and equivalent potential temperatures, (c) vertical velocity, (d) water vapor mixing ratio and the relative humidity, (e) cloud water/ice mixing ratio, and (f) the anomalies of potential temperature.

Ritchie and Elsberry (2001) used a mesoscale numerical model to study the transition of tropical cyclones to extratropical cyclones. Under ideal baroclinic conditions, a tropical cyclone undergoing a transformation develops a low-level warm anomaly to the west-southwest of the cyclone, which has similar characteristics to the pressure dip. The results of this study and of Ritchie and Elsberry's (2001) study demonstrate that a tropical cyclone undergoing transformation within mid-latitude large-scale atmospheric conditions generates a dip-like structure in surface pressure. Thus, we may say that a pressure dip is a unique phenomenon intrinsic to the transition of a tropical cyclone, although not every transforming typhoon is accompanied by the development of a pressure dip.

Pressure dips reported in previous studies are associated with typhoons that crossed Japan during September and October (e.g., Nakajima et al. 1980), with the exception of Typhoon Della that made landfall in June 1949 (Fujita 1952). Even during June and early-July a typhoon occasionally approaches Japan under the atmospheric conditions described above. The frequency of typhoons crossing Japan is greatest in late July and August, but pressure dips are not observed during summer when the westerly winds retreat to the north of Japan. This suggests that pressure dips tend to occur when a typhoon enters the zone of mid-latitude westerlies. These atmospheric conditions described above might be favorable for the transformation of the typhoon structure, e.g. extratropical transition (Muramatsu 1982; Kitabatake 2002). Actually, the typhoons with pressure dips were of considerable intensity at the time they approached the Japan Islands, and then weakened rapidly and eventually transformed into extratropical cyclones during their passage over the Japan Islands.

Fujita (1992) noticed that there were two types of pressure dips in their analyzing U.S. hurricanes and Japanese typhoons: (a) cold-sector dip which forms in the wake of a rainband in the northwest sector, and (b) warm-sector dip which forms in any sector of storms free cold-air inflow. The former types are similar to the characteristic of our focused pressure dips, while the latter types seems to correspond to pressure dips that we exclude in the present study. However, because of limitation of our available data, the characteristic of pressure dips associated with hurricanes is not clear, and this reminds the future work.

7. Summary

We simulated the pressure dips associated with Typhoon Zeb using a mesoscale numerical model. The model successfully reproduced the features of pressure dips, and then we investigated the formation process of the pressure dips.

The simulated pressure dips are closely linked to warm potential temperature anomalies in the lower troposphere. Accompanied by the anomalies, the relative humidity and rainwater are less, while there is the overhanging anvil characterized by abundant snow and cloud ice above the melting level over there. As the typhoon moves into the mid-latitude westerlies, a dry air carried by the mid-latitude westerlies enters the anvil with getting the negative buoyancy through evaporative cooling, resulting in the formation of downdraft. The parcels undergo acceleration through evaporation until it goes through the melting level. Below the melting levels where there is less hydrometer, however, evaporative cooling is insufficient to offset the adiabatic warming. As a result, the warm potential temperature anomalies are caused in the lower level, resulting in the formation of pressure dips. The horizontal scale of pressure dips is set by the width of the region of mesoscale downdraft around the melting level.

The pressure dips were observed under the large-scale environmental conditions characterized by the westerly winds associated with a mid-latitude trough with a dry air mass to the west of Japan at upper levels and cold fronts at lower levels. The pressure dips are detected in the typhoon in boreal fall when the above large-scale environmental conditions appear around Japan. No pressure dip is observed in boreal summer when typhoons mostly approach toward Japan. We therefore suggest that a pressure dip is an inherent feature of the asymmetric structure of a typhoon undergoing extratropical transition.

Acknowledgments.

We are grateful for the efforts of many scientists at both PSU and NCAR to maintain MM5 and acknowledge the Meteorological Research Institute and Japan Meteorological Agency for supplying meteorological data of past tropical cyclones. This work is partly supported by the Research Project for Suitable Coexistence of Human, Nature, and the Earth under the Japanese Ministry of Education, Sports, Culture, Science, and Technology.

References

Anthes, R., E. –Y.Hsie, and Y.–H. Kuo, 1987: Description of the Penn state/NCAR Mesoscale model version 4 (MM4). [Available from NCAR publications office, P.O. box 3000, boulder, co 80307–3000.], *NCAR Tech. Note NCAR/TN–282*, 66 pp.

Dudhia, J., 1989: Numerical study of convection observed during the winter monsoon experiment using a mesoscale two-dimensional model. *J. Atmos. Soc*., **46**, 3077–3107.

—, 1993: A nonhydrostatic version of the Penn State–NCAR mesoscale model: Validation tests and simulation of an Atlantic cyclone and cold front). *Mon. Wea. Rev*., **121**, 1493–1513.

Fudeyasu, H. and O, Tsukamoto, 2000: Pressure Dip Observed in the Typhoon 9810, *Tenki*, **47**, 37–451. (in Japanese).

Fujii, T., 1992: Meteorological Characteristics of High Wind of Typhoon 9119 (MIREILLE). J*. Wind Eng.,* **53**, 27–35. (in Japanese).

Fujita, T., 1952: Study on pressure dips within typhoon Della. *Bull. Kyushu Inst. Technol*., **2**, 52–61.

—, 1992: Japanese Typhoons, Mystery of Severe Storms, *Univ. of Chicago*, 144–150.

Gallus, W. A. Jr., 1996: The influence of micrphysics in the formation of intense wake lows: A numerical modeling study. *Mon. Wea. Rev*., **124**,

2267–2281.
Grell, G. A., 1993: Prognosic evaluation of assumptions used by cumulus parameterizations. *Mon. Wea. Rev*., **121**, 764–787.
—, J. Dudhia, and D. R. Stauffer, 1995: A description of the fifth generation Penn State/NCAR mesoscale model (MM5). [Available from NCAR Publications Office, P.O. Box 3000, Boulder, CO 80307–3000.], *NCAR Tech Note NCAR/TN–398+STR*, 138 pp.
Hong, S.–Y., and H.–L. Pan, 1996: Nonlocal boundary layer vertical diffusion in a medium-range forecast model. *Mon. Wea. Rev*., **124**, 2322–2339.
Inoue, T., K. Yoshida, A. Tabata., H. Tanaka and K. Sakamoto, 1999: A sharp pressure dip observed in the Typhoon T9810 (Zeb).*Bull. Kobe Marrin Obs*., **218**, 1–10. (in Japanese).
Johnson, R. H., and P. J. Hamilton, 1988: The relationship of surface pressure features to the precipitation and airflow structure of an intense midlatitude squall line. *Mon. Wea. Rev*., **116**, 1444–1472.
Kalnay, E., M. Kanamitsu., R. Kistler, W. Collins, D. Deaven, L. Gandin, M. Iredell, S. Saha, G. White, J. Wollen, Y. Zhu, M. Chelliah, W. Ebisuzaki, J. Wang, A. Leetmaa, R. Reynolds, R. Jenne and D. Joseph, 1996: The NCEP/NCAR 40-year reanalysis project. *Bull. Amer. Meteor. Soc.*, **77**, 437–471.
Kitabatake, N., 2002: Extratropical Transformation of Typhoon Vicki (9807): Structural Change and the Role of Upper-tropospheric Disturbances. *J. Meteor. Soc. Japan*, **80**, 229–247.
Maeda, H., 1994: On the Pressure dip within Typhoon 9119. J. *Meteor. Res*., **46**, 25–38. (in Japanese).
Matsumoto, S. and H. Okamura, 1985: The Internal Gravity Wave Observed in the Typhoon T8124 (Gay). *J. Meteor. Soc. Japan*, **63**, 37–51.
Muramatsu, T., 1982: Extratropical transformation of mature typhoon: The case study of Typhoon 7916, Owen. *Tenki*, **29**, 1199–1212. (in Japanese)
Miller, M. J., and A. K. Betts, 1977: Trave;ing convective storms over Venezuela. *Mon. Wea. Rev*., **105**, 838–848.
Nakajima, C., Y. Mitsuta, Y. Gocho, M. Tanaka, T. Fujii and N. Monji., 1980: On Typhoon 7916. *Disas. Prev. Res. Inst., Kyoto Univ. Annual.*, **23**, 87–111. (in Japanese).
Obayashi, M., 1991: Data processing in the system for very short-range forecast of precipitation (in Japanese). *Sokko-Jihou,* **58,** 189-207.
Ritchie E. A. and R. L. Elsberry, 2001: Simulations of the Transformation Stage of the Extratropical Transition of Tropical Cyclones. *Mon. Wea. Rev*., **129**, 1426–1480.
Schmidt, J. M., and W. R. Cotton, 1990: Interactions between upper and lower troposphere gravity waves on squall line structure and maintenance. *J. Atmos. Sci.*, 47, 1205-1222.
Tsujimura. Y., 1993: Meteorology, soliton and modon. *Meteor. Res. Note*.**178**, 73–79. (in Japanese).
Zhang, D.-L., and K. Gao, 1989: Numerical simulations of an intense squall line during 10-11 June 1985 PRE-STORM. Part II: Rear inflow, surface pressure perturbations and stratiform precipitation. *Mon. Wea. Rev*., **117**, 2067–2094.